Journal of Alloys and Compounds 494 (2010) 410–414

Contents lists available at ScienceDirect

Journal of Alloys and Compounds

journal homepage: www.elsevier.com/locate/jallcom

Synthesis of nickel and nickel oxide nanoparticles via heat-treatment of simple octanoate precursor

Masoud Salavati-Niasari [a,b,*], Fatemeh Davar [a,*], Zeinab Fereshteh [a]

[a] *Institute of Nano Science and Nano Technology, University of Kashan, Kashan, P.O. Box 87317-51167, Islamic Republic of Iran*
[b] *Department of Inorganic Chemistry, Faculty of Chemistry, University of Kashan, Kashan, P.O. Box 87317-51167, Islamic Republic of Iran*

ARTICLE INFO

Article history:
Received 15 November 2009
Received in revised form 11 January 2010
Accepted 12 January 2010
Available online 21 January 2010

Keywords:
Nanostructures
NiO
Chemical synthesis
Magnetic properties

ABSTRACT

Nickel oxide nanoparticles have been synthesized via heat-treatment of a new precursor nickel octanoate Ni(octa)$_2$; (octa = octanoate); in the range of 400–900 °C. The effect of calcination temperature on particle size has been investigated. When the calcinations were conducted in air from 400 to 900 °C, the precursor Ni(octa)$_2$ was first changed to Ni, then to NiO. When calcined in argon atmosphere, Ni(octa)$_2$ was directly converted into pure Ni at as low as 500 °C. The products were characterized by X-ray diffraction (XRD), scanning electron microscopy (SEM), transmission electron microscopy (TEM) and Fourier transform infrared (FT-IR) spectroscopy. The synthesized NiO nanoparticles have quasi-spherical particles with size of about 24 nm. The optical absorption band gap of NiO nanoparticles is 3.41 eV.

1. Introduction

Recently, nanomaterials have attracted extensive interest because of their unique properties in various fields in comparison with their bulk counterparts [1]. A reduction in particle size to nanometer scale results in various interesting properties compared with their bulk properties. Having a large surface area, metal oxide nanomaterials show great advantages over conventional materials in many applications. Nickel oxide is an antiferromagnetic material that has a wide range of technological applications at the nanoscale.

For example, NiO nanoparticles have been found to be promising as an electrode material for lithium ion batteries [2]. Nanosized NiO has demonstrated excellence properties such as catalytic [3], magnetic [4], electrochromic [5], optical and electrochemical properties [3]. Furthermore, nickel oxides can be used as a transparent p-type semiconducting layer [6] and are being studied for applications in smart windows, electrochemical supercapacitors [7] and dye-sensitized photocathodes [8]. For technological applications, a detailed understanding of the size, morphology and interparticle interactions of nanoscale NiO could be important [9].

A great many methods have been employed to synthesize NiO nanoparticles such as evaporation [10], electrodeposition [11], thermal decomposition [12] and sol–gel techniques [13].

Recently Shah reported synthesis of 50–60 nm nickel oxide nanoparticles after 12 h using sonication and hydrothermal methods [14]. More recently the NiO nanoparticles were synthesized using two different microemulsion approaches by Palanisamy and Raichur. It was reported that Ni(OH)$_2$ particles were first formed, then calcined at 600 °C to obtain 47 nm nickel oxide NiO particles [15]. Song and Gao synthesized NiO nanorods consisting of numerous NiO nanoparticles by thermal decomposition of rod-like nickel oxide precursor achieved by microwave-assisted method [16]. Rodríguez-Llamazares et al. synthesized nickel/nickel oxides nanoparticles by a method based on ligand displacement of bis(1,5-cyclooctadiene)-nickel(0), zerovalent organometallic precursor and simultaneous formation of a thiourea inclusion compound [17]. Nickel oxide nanoparticles have been synthesized via decomposition of nickel oxalte NiC_2O_4 at 450 °C [2]. Thermal decomposition method has some advantages such as simple process, low cost and easiness to obtain high purity products hence it is quite promising and facile route for industrial applications.

In our group, we have been interested for a few years in the synthesis of metal, metal oxide and metal sulfide nanoparticles, using new inorganic precursor, taking profit of the tools of organometallic chemistry [18–22]. A major interest at the moment is in the development of organometallic or inorganic compound for preparation of nanoparticles [23–25]. Using of the novel compound can be useful and open a new way for preparing nanomaterials to control nanocrystal size, shape and distribution size.

---

* Corresponding authors at: Institute of Nano Science and Nano Technology, University of Kashan, Kashan, P.O. Box 87317-51167, Islamic Republic of Iran.
Tel.: +98 361 5555333; fax: +98 361 5552935.
E-mail addresses: salavati@kashanu.ac.ir (M. Salavati-Niasari), davar@kashanu.ac.ir (F. Davar).

0925-8388/$ – see front matter © 2010 Elsevier B.V. All rights reserved.
doi:10.1016/j.jallcom.2010.01.063

Table 1
Reaction conditions and corresponding products.

Reaction temperature (°C)	Reaction time (h)	Reaction atmosphere	Composition of the products (XRD result)
300	3	Air	NiO + $Ni(octa)_2$ (main)
350	4	Air	NiO + $Ni(octa)_2$ (minor)
400	4	Air	NiO (main) + Ni (minor)
500–900	4	Air	NiO
350	4	Ar	Ni (main) + $Ni(octa)_2$ (minor)
400	4	Ar	Ni
500–800	4	Ar	Ni

Herein, we report a systematic synthesis of Ni and NiO nanoparticles via the heat-treatment of $Ni(octa)_2$ precursors, which were prepared through a simple precipitation method. In this process, pure NiO nanoparticles were synthesized without any surfactant and solvent by dry, simple method. To the best of our knowledge, this is the first report on the synthesis of NiO nanoparticles from $Ni(octa)_2$; (octa = octanoate). The aim of the present work is to prepare nanocrystals of NiO using thermal decomposition method and its physicochemical characterization.

2. Experimental

2.1. Materials

All the chemical reagents used in our experiments were of analytical grade and were used as received without further purification. Octanoic acid, nickel nitrate, NaOH and ethanol were purchased from Aldrich and used as received.

2.2. Characterization

XRD patterns were recorded by a Rigaku D-max C III, X-ray diffractometer using Ni-filtered Cu Kα radiation. Elemental analyses were obtained from Carlo ERBA Model EA 1108 analyzer. Scanning electron microscopy (SEM) images were obtained on Philips XL-30ESEM equipped with an energy dispersive X-ray spectroscopy. Transmission electron microscopy (TEM) images were obtained on a Philips EM208 transmission electron microscope with an accelerating voltage of 100 kV. X-ray photoelectron spectroscopy (XPS) of the as-prepared products was measured on an ESCA-3000 electron spectrometer with nonmonochromatized Mg Kα X-ray as the excitation source. Fourier transform infrared (FT-IR) spectra were recorded on Shimadzu Varian 4300 spectrophotometer in KBr pellets. Mass spectrum (MS) was measured with a JMS-700 (JEOL Ltd.) operated in a negative ion mode. The sample for MS was mixed in diethanolamine as a matrix. The elemental analysis (carbon and hydrogen) of the materials was obtained from Carlo ERBA Model EA 1108 analyzer. The electronic spectra of the complexes were taken on a Shimadzu UV–vis scanning spectrometer (Model 2101 PC). The magnetic measurement was carried out in a vibrating sample magnetometer (VSM) (BHV-55, Riken, Japan) at room temperature.

2.3. Synthesis of nickel octanoate ($Ni(octa)_2$)

Five gr of NaOH was dissolved into 5 mL deionized water and 10 mL absolute ethanol then soda solution was introduced into 2.5 g of octanoic acid under continuous stirring for about 2 h. Then 15 mL deionized water was introduced into the above solution and was put on ice bath and was added below solution (15 g NaCl was dissolved into 100 mL deionized water), in the result, white precipitate was formed after 10 min, this precipitate was filtrated and was washed by cool deionized water then was dried. This white precipitate is sodium octanoate (Na(octa)). Sodium octanoate (24 mmol) was completely dissolved in deionized water (50 mL). Nickel(II) nitrate (12 mmol) in deionized water (10 mL) was added to the solution. A deep green precipitate was formed after 2 h reflux. The precipitate was collected by filtration and washed with deionized water. Then, the solid was reprecipitated by adding MeOH. The precipitate was dried in oven in 50 °C for 5 h. Analytical data. FAB-MS: $m = z$ 344.7 [M^-]; analytical calculations for $C_{16}H_{30}O_4Ni$ consist: C, 55.69; H, 8.76; Ni, 17.01%. Found: C, 55.72; H, 8.79; Ni, 17.05%; IR (FT-TR method): 2922 (CH_3), 2854 (CH_2), 1589 (COO), 1470–1415 (CH_3, CH_2), 722 (OCO) cm^{-1}.

2.4. Preparation of Ni and NiO nanoparticles

The as-prepared $Ni(octa)_2$ precursor was subsequently calcined in the temperature range of 300–900 °C in a furnace for 4 h to get nickel oxide. In parallel, pure Ni nanoparticles were also prepared through calcining $Ni(octa)_2$ precursor under flowing argon atmosphere at 350–800 °C for 4 h (see Table 1).

3. Results and discussion

Fig. 1a–f shows the XRD patterns of the products prepared through heating $Ni(octa)_2$ in air at 400–900 °C for 4 h, respectively. The diffraction peaks in pattern a can be indexed to cubic Ni and cubic phase of NiO. The diffraction peaks in patterns b–f can be indexed to pure NiO cubic phase. Fig. 1h is the XRD pattern of the product resulted from heating $Ni(octa)_2$ in Ar at 400 °C for 4 h. All diffraction peaks can be indexed to pure cubic Ni. The peaks are extremely broad. Three characteristic peaks at 44.3°, 52.1°, 76.6° for face-centered cubic (fcc) nickel (JCPDS, no. 01-1260) marked by their indices (1 1 1), (2 0 0) and (2 2 0) were observed. This revealed that the as-synthesized nanocrystals were pure nickel.

The crystallite sizes of the as-synthesized nickel, D_c, was calculated from the major diffraction peaks of the base of (1 1 1) using

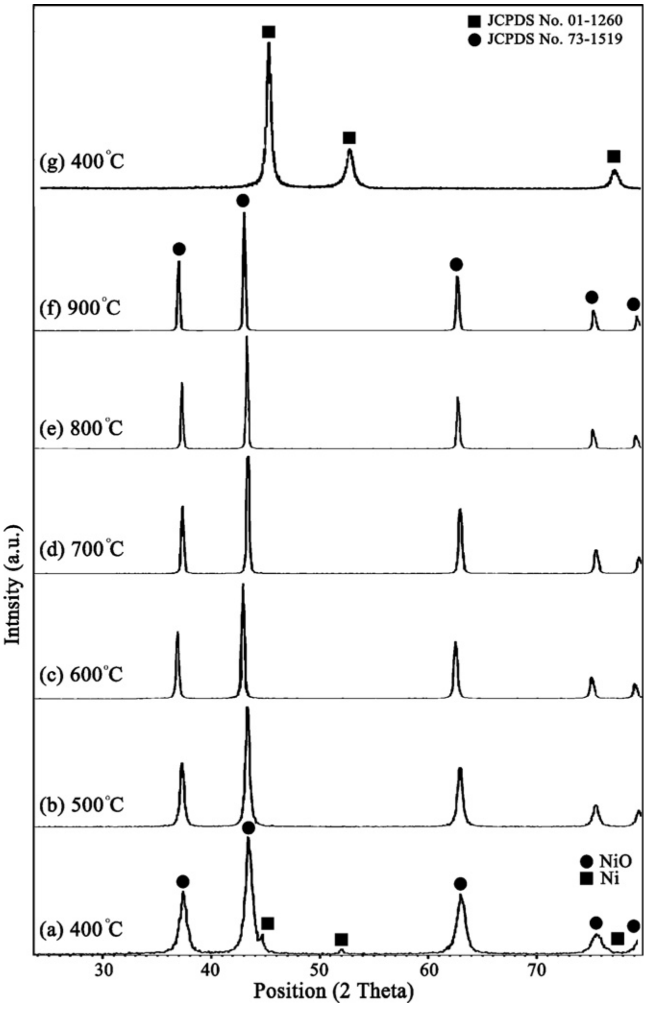

Fig. 1. XRD patterns of the as-prepared nanoparticles calcined at different temperatures.

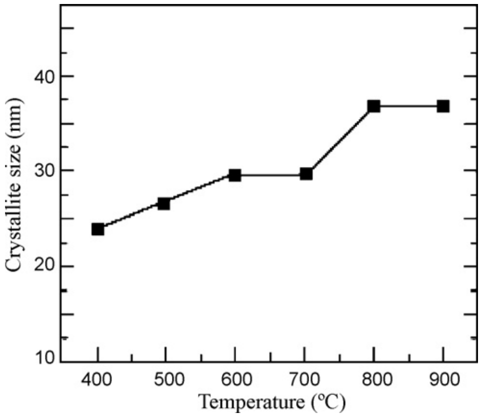

Fig. 2. Evolution of crystallite size of NiO powders calcined at different temperatures.

the Scherrer formula (Eq. (1)),

$$D_c = \frac{K\lambda}{\beta\ \cos\theta} \quad (1)$$

where K is a constant (ca. 0.9) [26], λ is the X-ray wavelength used in XRD (1.5418 Å), θ is the Bragg angle and β is the pure diffraction broadening of a peak at half-height, that is, broadening due to the crystallite dimensions. The diameter of the nanoparticles calculated by the Scherrer formula is 24 nm.

The evolution of the crystal size (D_c) of the NiO prepared at different calcination temperatures is shown in Fig. 2. The data show that the growth in crystallite size of nickel oxide has a strong relationship with the sintering temperature. The crystallite size NiO increase linearly until the calcination temperature reaches 700 °C. The size of NiO also increases linearly from 24 nm (400 °C) to 29 nm (700 °C). After 700 °C, the crystallite size of nickel oxide significantly increases to 36 nm at 800 °C and at higher calcination temperatures (>800 °C) shows no significant change in crystallite size, which is 36 nm.

The surface morphological study of the nickel oxide nanoparticles was carried out using SEM image. Fig. 3a shows the SEM image of the prepared NiO at 500 °C in air for 4 h. From the SEM analyses, one can conclude the formation of nanoparticles spherical structure (Fig. 3a). The transmission electron microscopic (TEM) photographs of the product has been given in Fig. 3b. The size of nanoparticles obtained from the XRD diffraction patterns are in close agreement with the TEM studies which show sizes of 20–30 nm.

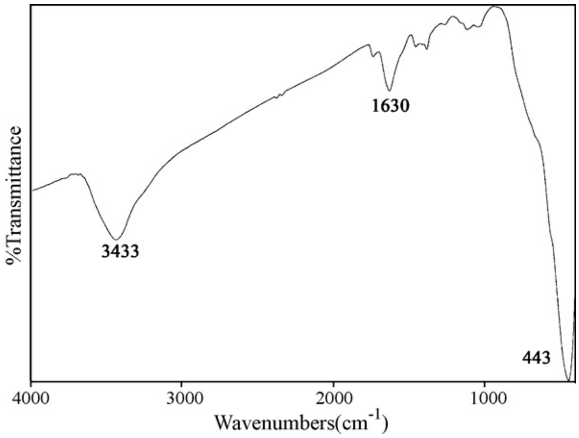

Fig. 4. FT-IR spectra of NiO nanoparticles calcined at 500 °C in air for 4 h.

FT-IR spectroscopy is a useful tool to understand the functional group of any organic molecule (Fig. 4). Metal oxides; NiO; generally give absorption bands below 1000 cm^{-1} arising from inter-atomic vibrations. The peak at 443 cm^{-1} in spectrum, showing Ni–O bond, gave clear evidence about the presence of the crystalline NiO [27]. The board peak at 3433 cm^{-1} in spectra is representative of H_2O. Also, the H–OH bending vibration appears at 1635 cm^{-1}. There was no evidence of free precursor, nickel octanoate, in the sample, because stretch vibration of C=O ($\upsilon_{C=O}$) and C–O (υ_{C-O}) disappeared. About prepared samples in Ar atmosphere the absorption peak below 1000 cm^{-1} were not observed. So we can say that FT-IR spectra agree with XRD patterns, which shows that obtained samples under Ar atmosphere are pure metallic nickel and not oxidized. But it is clear that the surface of these samples is oxidized because the sample was exposed to air. After being oxidized under air, new peak is appeared at about 450 cm^{-1}, that this peak was undoubtedly assigned to Ni–O stretching as was reported at literature.

Further evidence for the purity and composition of the products was obtained by X-ray photoelectron spectra (XPS). Fig. 5 shows the XPS of the prepared NiO nanoparticles at 500 °C in air for 4 h. The binding energies of Ni $2p_{1/2}$, Ni $2p_{3/2}$ and O 1s, provided a fairly complete picture of the sample powder. The Ni $2p_{3/2}$ XPS peak that appears at 855.4 eV coincides with the findings for NiO. The O 1s peak at 530.5 eV is attributed to the (O^{-2}) in the NiO.

Fig. 6 is the UV–vis spectrum of the as-synthesized NiO nanoparticles dispersed in ethanol. A strong absorption in the UV region is

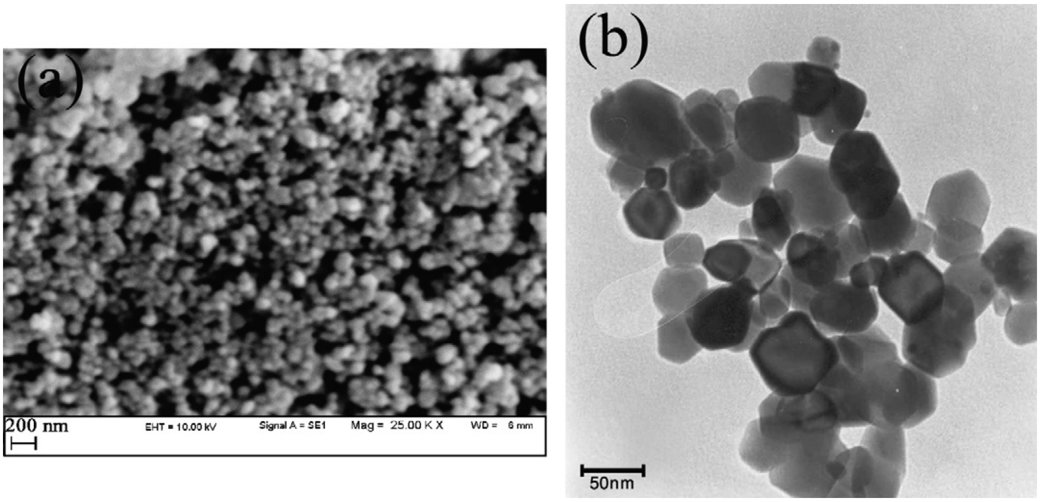

Fig. 3. SEM and TEM images of the prepared NiO at 500 °C in air for 4 h.

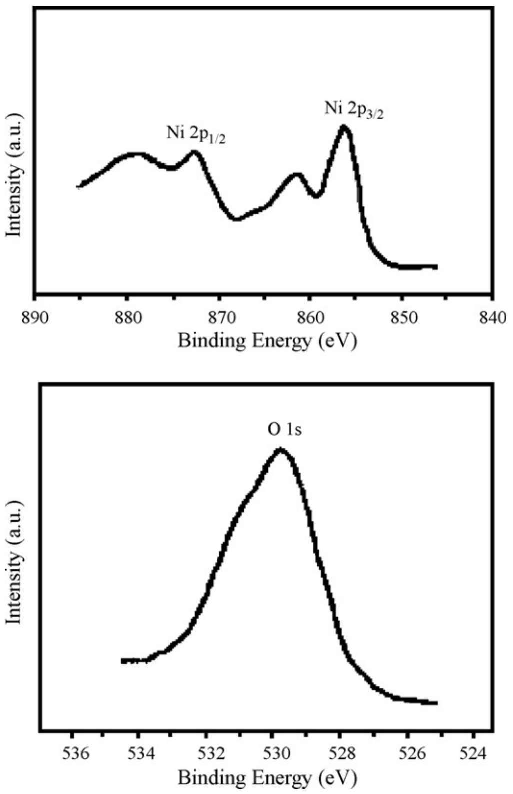

Fig. 5. XPS spectra of the NiO nanoparticles.

observed at wavelengths about 364 nm. The strong absorption in the UV region is attributed to band gap absorption in NiO [28]. It is well known that optical band gap (E_g) can be calculated on the basis of the optical absorption spectrum by the following equation:

$$(Ah\nu)^n = K(h\nu - E_g)$$

where $h\nu$ is the photo energy, A is absorbance, K is a constant relative to the material and n is either two for direct transition or 1/2 for an indirect transition [29]. Hence, the optical band gap for the absorption peak can be obtained by extrapolating the linear portion of the $(Ah\nu)^2$–$h\nu$ curve to zero. The band gap is determined by extrapolating the linear portion of the plot to the energy axis. The band gap of the NiO particles is about 3.41 eV. Reported band gap energies for NiO are in the range 3.4–3.8 eV [30], which is in good agreement with our report. The value of band gap of the NiO nanoparticles is about 3.41 eV, which is smaller than the value of bulk material. It is well known that semiconductors with nanoscale size show a blue shift in their spectra due to the quantum confinement effects. However, the as-obtained samples have an E_g smaller than the bulk one. This effect is likely due to the chemical defects or vacancies present in the intergranular regions generating new energy level to reduce the band gap energy [16].

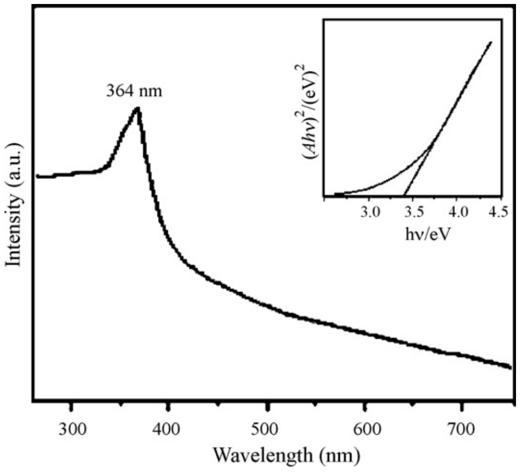

Fig. 6. UV–vis absorption spectrum and $(Ah\upsilon)^2$ vs. $h\upsilon$ curve (inset) for NiO nanoparticles calcined at 500 °C.

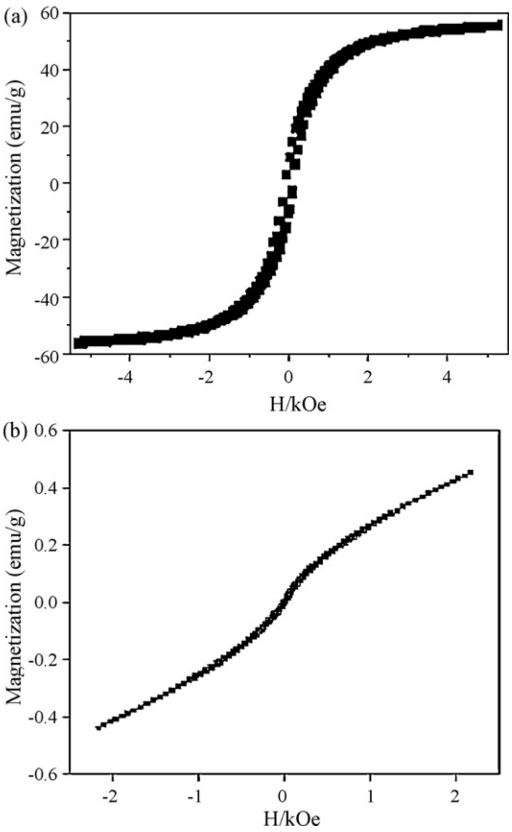

Fig. 7. Magnetization versus applied at 300 K for (a) Ni and (b) NiO nanoparticles.

No linear relation was found for $n = 1/2$, suggesting that the as-prepared NiO nanoparticles are semiconducting with direct transition at this energy [28].

The magnetic property of Ni nanoparticles (obtained sample at 500 °C in argon atmosphere) has been measured (Fig. 7a). The saturation magnetization (M_s) for the nanoparticles is 55.7 emu g^{-1} (1 emu g^{-1} = 1 A m^2 kg^{-1}) which is close to that of bulk Ni (ca. 55 Oe (1 Oe = 79.6 A m^{-2})). Coercivity field (H_c) of Ni nanoparticles is about (90 Oe) [31]. Compared with the corresponding value for bulk Ni, the coercivities of the Ni nanoparticles clearly show significant enhancement. This enhancement can probably be attributed to the reduced particle sizes of obtained product [32] which change the magnetization reversal mechanism. This demonstrates that the magnetic properties of the Ni nanoparticles are greatly influenced by their microstructure. The hysteresis loop of the Ni indicates a ferromagnetic behavior. As shown in the Fig. 7a, the hysteresis loop is symmetric with respect to zero magnetic fields, indicating that there is no exchange biasing effect, which is usually caused by the presence of NiO [33,34]. Fig. 7b shows the hysteresis loops of NiO nanoparticles at 300 K. It can be seen that NiO nanoparticles present a superparamagnetic behavior although NiO bulk material is antiferromagnetic [35].

4. Conclusion

Nickel and nickel oxide nanoparticles with size about of 24 nm have been successfully prepared via a simple heat-treatment of nickel octanoate as a new precursor. The magnetic coercivity of Ni nanoparticles is as high as 90 Oe. This method is nontoxic, facile and inexpensive. This work is easily extended to other metals.

Acknowledgements

Authors are grateful to the Council of Iran National Science Foundation and University of Kashan for their unending effort to provide financial support to undertake this work.

References

[1] C.C. Chen, A.B. Herhold, C.S. Johnson, A.P. Alivisatos, Science 276 (1997) 398–401.
[2] X. Wang, J. Song, L. Gao, J. Jin, H. Zheng, Z. Zhang, Nanotechnology 16 (2005) 37–39.
[3] D. Wang, R. Xu, X. Wang, Y. Li, Nanotechnology 17 (2006) 979–983.
[4] Y.R. Uhma, J.H. Park, W.W. Kima, C.H. Chob, C.K. Rhee, Mater. Sci. Eng. B 106 (2004) 224–227.
[5] S.H. Lin, F.R. Chen, J.J. Kai, Appl. Surf. Sci. 254 (2008) 3357–3363.
[6] H. Sato, T. Minami, S. Takata, T. Yamada, Thin Solid Films 236 (1993) 27–31.
[7] V. Srinivasan, J. Weidner, J. Electrochem. Soc. 144 (1997) L210–L213.
[8] J. He, H. Lindström, A. Hagfeldt, S.E. Lindquist, J. Phys. Chem. B 103 (1999) 8940–8943.
[9] P. Poizot, S. Laruelle, S. Grugeon, L. Dupont, J.-M. Tarascon, Nature 407 (2000) 496–499.
[10] R. Cinnsealach, G. Boschloo, S.N. Rao, D. Fitzmaurice, Sol. Energy Mater. Sol. Cells 57 (1999) 107–125.
[11] C. Natarajan, H. Matsumoto, G. Nogami, J. Electrochem. Soc. 144 (1997) 121–126.
[12] C.S. Carney, C.J. Gump, A.W. Weimer, Mater. Sci. Eng. A 431 (2006) 1–12.
[13] A. Surca, B. Orel, B. Pihlar, P. Bukovec, J. Electroanal. Chem. 408 (1996) 83–100.
[14] M.H. Shah, Nanoscale Res. Lett. 3 (2008) 255–259.
[15] P. Palanisamy, A.M. Raichur, Mater. Sci. Eng. C 29 (2009) 199–204.
[16] X. Song, L. Gao, J. Am. Ceram. Soc. 91 (2008) 3465–3468.
[17] S. Rodríguez-Llamazares, J. Merchán, I. Olmedo, H.P. Marambio, J.P. Muñoz, P. Jara, J.C. Sturm, B. Chornik, O. Peña, N. Yutronic, M.J. Kogan, J. Nanosci. Nanotechnol. 8 (2008) 3820–3827.
[18] M. Salavati-Niasari, F. Davar, M. Mazaheri, Mater. Lett. 62 (2008) 1890–1892.
[19] M. Salavati-Niasari, F. Davar, Mater. Lett. 63 (2009) 441–443.
[20] M. Salavati-Niasari, F. Davar, M. Mazaheri, Mater. Res. Bull. 44 (2009) 2246–2251.
[21] M. Salavati-Niasari, N. Mir, F. Davar, J. Alloys Compd. 476 (2009) 908–912.
[22] M. Salavati-Niasari, Z. Fereshteh, F. Davar, Chem. Eng. J. 146 (2009) 498–502.
[23] N. Bouropoulos, G.C. Psarras, N. Moustakas, A. Chrissanthopoulos, S. Baskoutas, Phys. Status Solidi A 205 (2008) 2033–2037.
[24] S. Baskoutas, P. Giabouranis, S.N. Yannopoulos, V. Dracopoulos, L. Toth, A. Chrissanthopoulos, N. Bouropoulos, Thin Solid Films 515 (2007) 8461–8464.
[25] M. Salavati-Niasari, F. Davar, M. Mazaheri, J. Alloys Compd. 470 (2009) 502–506.
[26] H.P. Klug, L.E. Alexander, X-ray Diffraction Procedures for Polycrystalline and Amorphous Materials, second ed., Wiley, New York, 1974.
[27] M. Kanthimathi, A. Dhathathreyan, B.V. Nair, Mater. Lett. 58 (2004) 2914–2917.
[28] X. Li, X. Zhang, Z. Li, Y. Qian, Solid State Commun. 137 (2006) 581–584.
[29] A. Hagfeldt, M. Gratzel, Chem. Rev. 95 (1995) 49–68.
[30] B. Sasi, K.G. Gopchandran, Nanotechnology 18 (2007) 115613–115621.
[31] Y. Mi, D. Yuan, Y. Liu, J. Zhang, Y. Xiao, Mater. Chem. Phys. 89 (2005) 359–361.
[32] J.H. Hwang, V.P. Dravid, M.H. Teng, J.J. Host, B.R. Elliott, D.L. Johnson, T.O. Mason, J. Mater. Res. 12 (1997) 1076–1082.
[33] C. Liu, L. Guo, R. Wang, Y. Deng, H. Xu, S. Yang, Chem. Commun. (2004) 2726–2727.
[34] J. Nogués, I.K. Schuller, J. Magn. Magn. Mater. 192 (1999) 203–232.
[35] P. Ngo, P. Bonville, M.P. Pileni, Eur. Phys. J. B 9 (1999) 583–593.